Numerical simulation of concrete dynamic response using RHT material model

DAN ILIE BULIGA[1]

Abstract*: Sophisticated numerical models are increasingly used to analyze complex physical processes such as concrete structures subjected to high-impulsive loads. Among other influencing factors for a realistic and reliable analysis, it is essential that the material models are capable of describing the material behavior at the pertinent scale level in a realistic manner. One of the widely used concrete material models in impact and penetration analysis, the RHT model, covers essentially all macro features of concrete-like materials under high strain rate loading. With the implementation in AUTODYN, the RHT model has been widely used in the modeling of concrete-like brittle materials for high-impulsive response analysis such as impact and penetration.*

Keywords*: numerical models, concrete structures, impact and penetration, RHT model.*

1. Introduction

Concrete is a common material used in civil and defense constructions. Modeling of the concrete behavior under static or quasi-static loading has been a subject of extensive studies for many decades. Modeling of the concrete behavior under high rate loading is relatively new and it has become a topic of wide attention in more recent years.

Adequate material constitutive modeling and sound computational techniques are both essential to a reliable numerical simulation of complex responses. For brittle materials like concrete, the macroscopic inelastic response stems from material fracture, buckling and crushing of the cement paste and aggregate micro-structure [1]. These mechanisms become even more complex under high loading rate conditions. It is difficult to model the microscopic mechanical processes in the analysis of a real life problem. Instead, the

[1] Military Technical Academy, 39-49 George Cosbuc Ave., Sector 5, 050141, Bucharest, Romania, dan.buliga@mta.ro

modeling of the material constitutive behavior for concrete-like materials is typically made at the macroscopic level that is consistent to the continuum description of the material using finite element methods. Nilsson [2] conducted some fundamental studies on the constitutive modeling of concrete subjected to high dynamic loads. A detailed description of the general modeling of concrete response using the theory of plasticity can be found in [3]. Recent advancements saw the development of several comprehensive concrete models that are aimed at high-impulsive load applications, with consideration of such effects as pressure hardening, strain hardening, material softening and rate-dependency. Models of this category include the RHT model [4,5,6], the K&C model [7,8] and JHC concrete model [9].

2. RHT concrete model

Material models that describe the mechanical response of the materials with an acceptable accuracy need to be included in FE codes to obtain accurate simulation results. Constitutive equations for concrete exposed to weapons effects have been a major area of interest for a long time, and several material models for concrete behavior have been developed. Furthermore, it is not until recent years that it has been possible to simulate the behavior of concrete targets during projectile penetration with acceptable results. One of the limitations for FE analyses of penetration in concrete structures has been the lack of validated material models for concrete subjected to the extreme loading conditions occurring during warhead impacts. The different tensile and compressive behavior of the concrete under high strain rate deformation, and with the need to consider the residual strength of the material under compression, require that a complex strength model is needed for the concrete during these loading conditions. One material model for FE codes which include these phenomena is the RHT concrete model.

The RHT model is described here with notations closely following the original documentation and implementation, with a thorough description of the model available in [4]. Furthermore, material parameters for normal strength concrete with a uniaxial compressive strength of 35 MPa were also given in the original documentation. The yield surfaces of the concrete for the material model are scaled with reference to the uniaxial compressive strength $c\ f$ for the concrete to obtain consequent data set for different concrete strengths. However, a new parameter set based on extensive material testing needs to be established if major changes of the behavior of the concrete are anticipated. Furthermore,

minor changes were introduced for the version of RHT material model implemented in the Autodyn, and these are noted in this description of the RHT material model. The background of the RHT model and its area of application are discussed by [5].

The description of the stress state in the material model relates to three pressure dependent yield surfaces for the definition of the elastic limit surface, failure surface and remaining residual strength surface for the crushed material, with the three yield surfaces described below. The failure surface can be seen as a function of the strength along the compression meridian $Y_{TXC}(p)$ multiplied by the factors $F_{Rate}(\dot{\varepsilon})$ and $R_3(\theta, Q_2)$ as:

$$Y^*_{TXC}(p) = \frac{Y_{TXC}(p)}{f_c} = A_{fail} + B_{fail}\left[p^* - HTL'^*\right]^{N_{fail}} \text{ for } p^* \geq \frac{1}{3} \qquad [4] \qquad \textbf{(1a)}$$

$$Y^*_{TXC}(p) = \frac{Y_{TXC}(p)}{f_c} = A\left[p^* - HTL'^*\right]^{N} \text{ for } p^* \geq \frac{1}{3} \qquad [10] \qquad \textbf{(1b)}$$

with A_{fail}, B_{fail} and N_{fail} are taken as material constants characteristic for the specific concrete. Furthermore, the intersection HTL' * normalised to f_c is defined by:

$$HTL'^* = \frac{1}{3} - \sqrt[N_{fail}]{\frac{1}{B_{fail}}} \qquad \text{with } HTL' = f_c \times HTL'^* \qquad \textbf{(2)}$$

Eqs. (1) and (2) above describes the high pressure compressive meridian, and are not used for pressure below $f_c/3$. Instead a piece-wise linear approximation of the compressive meridian is used between stress states representing the tensile strength (f_t/Q_2), the shear strength (f_t/Q_1) and the compressive strength according to *Figure 1*. The correction factors Q_1 and Q_1 are applied since the shear and uniaxial tensile stress states are located on the tensile and shear meridian, respectively. The reference points for the failure surface are shown in *Figure 2*, with a graphical representation of the correction factors shown later in *Figure 4a*.

The factor $F_{RATE}(\dot{\varepsilon})$ takes the strain rate enhancement into account according to:

$$F_{RATE}(\dot{\varepsilon}) = \begin{cases} \left(\dfrac{\dot{\varepsilon}}{\dot{\varepsilon}_0}\right)^{\alpha}, p \geq f_c/3, \dot{\varepsilon} = 30\times10^{-6}\,s^{-1} \\ \left(\dfrac{\dot{\varepsilon}}{\dot{\varepsilon}_0}\right)^{\delta}, p \geq -f_t/3, \dot{\varepsilon} = 3\times10^{-6}\,s^{-1} \end{cases} \qquad \textbf{(3)}$$

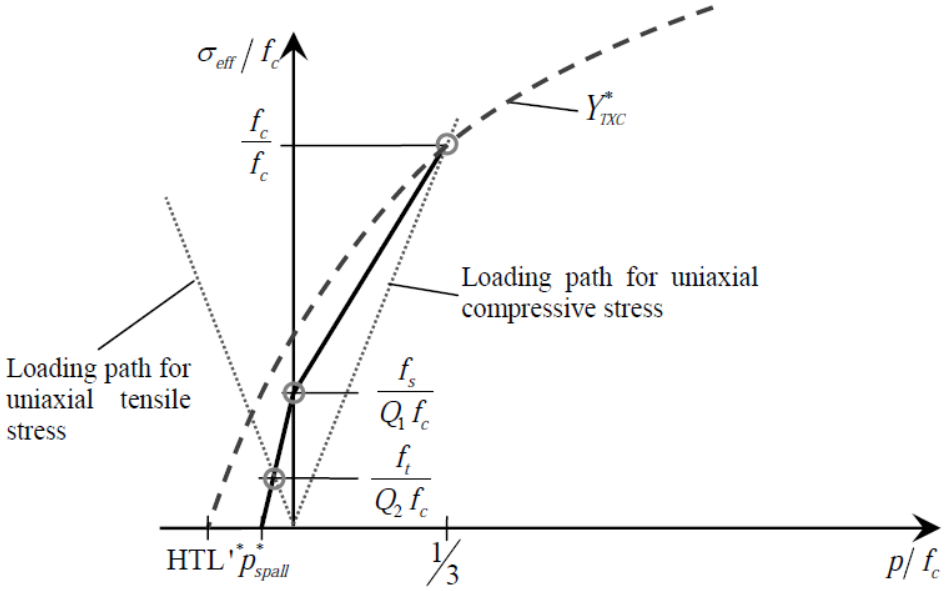

Figure 1. *The linear approximation of the compressive meridian at low pressures, modified from* [4] .

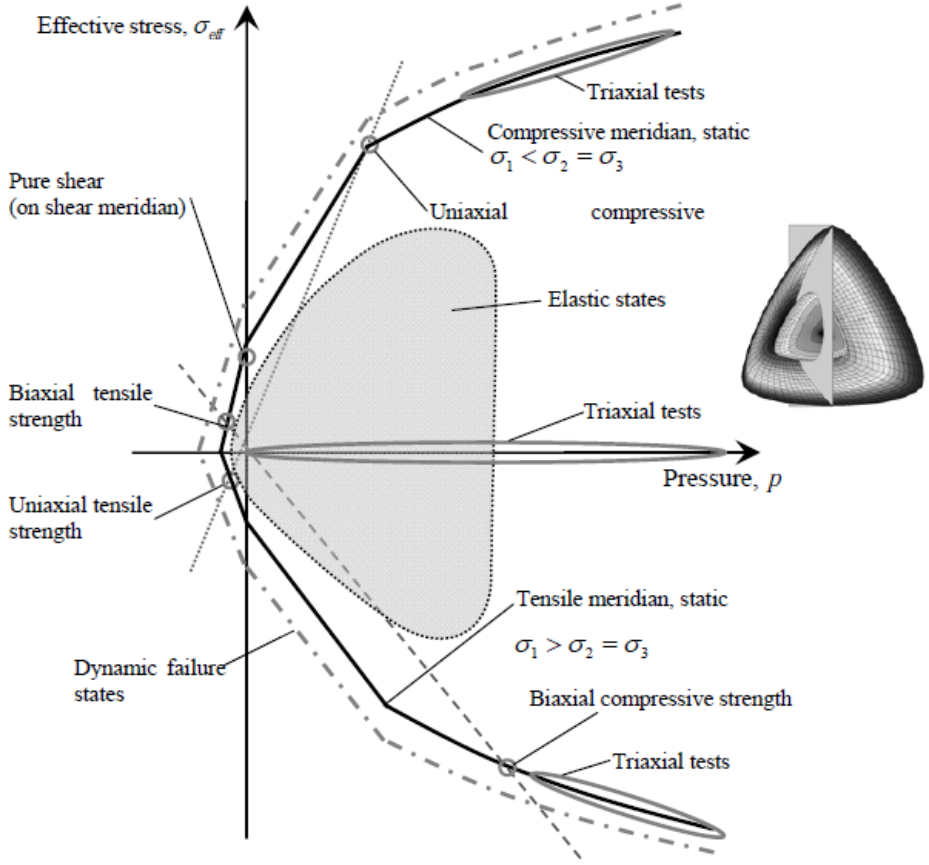

Figure 2. *A schematic figure of the reference points on the failure surface, modified from [4]. The insert shows the cut plane through the failure and elastic limit strength surfaces.*

Different strain rate enhancements are used for compressive and tensile loading conditions, with α and δ being material constants. Furthermore, the strain rate enhancement factor is linearly interpolated between the pressures $-f_t/3$ and $-f_c/3$. Testing of concrete at increased strain rates by using a split Hopkinson pressure bar (SHPB) have resulted in an increased dynamic compressive strength, e.g. the CEB-FIP model code [11] is suggesting a bilinear approximation of the strain rate enhancement factor both in tension and compression. This results in a rapid increase of the dynamic compressive strength according to the CEB-FIP model code at a strain rate greater than 30 s^{-1}. However, it seems that the major part of the dynamic increase of the compressive strain rate is related to the pressure dependent yield strength of concrete. The simulation of SHPB tests has shown that a pressure dependent constitutive model is likely to account for the major part of the dynamic increase of the compressive strength for concrete subjected to strain rates >30 s^{-1} [12].

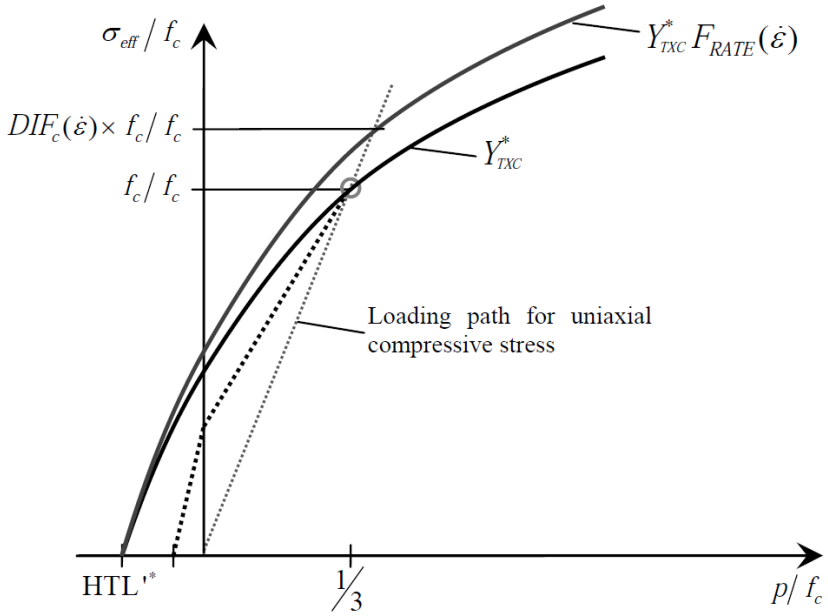

Figure 3. *The dynamic increase of the compressive meridian for $p \geq f_c/3$.*

The reduced failure strength for states off the compression meridian on the failure surface is introduced and given by the factor $R_3(\theta,Q_2)$. This factor scales the strength from the highest value at the compression meridian, and is given by:

$$R_3(\theta,Q_2)=\frac{2(1-Q_2^2)\cos\theta+(2Q_2-1)\left[4(1-Q_2^2)\cos^2\theta+5Q_2^2-4Q_2\right]^{\frac{1}{2}}}{4(1-Q_2^2)\cos^2\theta+(1-2Q_2)^2} \qquad \textbf{(4)}$$

Thus with θ rotating around the hydrostatic axis the entire failure surface can be calculated, see *Figure 4a*. The parameter Q_2 gives the distance from the hydrostatic axis to the tensile meridian divided by the distance between the hydrostatic axis to the compressive meridian as:

$$0.5 \le Q_2 = Q_{2,0} + BQ \times p^* \le 1 \tag{5}$$

The extreme case of Q_2 equal to 0.5 is found at low pressures and gives a triangular failure surface in the deviatory plane. At the other extreme Q_2 is equal to 1, and this gives a circular cross section of the failure surface according to *Figure 4b*. Thus at large confining pressures the surface approaches the circular form, with the pressure dependence of Q_2 according to Eq. (5) above. This method to account for the reduced concrete strength of the compressive meridian was first used by William and Warnke [13]. Furthermore, the parameter Q_1 used for definition of the failure surface at low pressures relates the distance from the shear meridian to the hydrostatic axis to distance from the compressive meridian to the hydrostatic axis. The elastic limiting surface $Y_{el}(p, \theta, \dot{\varepsilon})$ shown in *Eq. (6)* and *Figure 5* is scaled from the failure surface by the scaling factor $Y_o F$ along the loading paths. This scaling factor varies linearly from $f_{c,el}/f_c$ to $f_{t,el}/f_t$ between the pressures $-f_{t,el}/3$ and $f_{c,el}/3$ according to *Fig 6*.

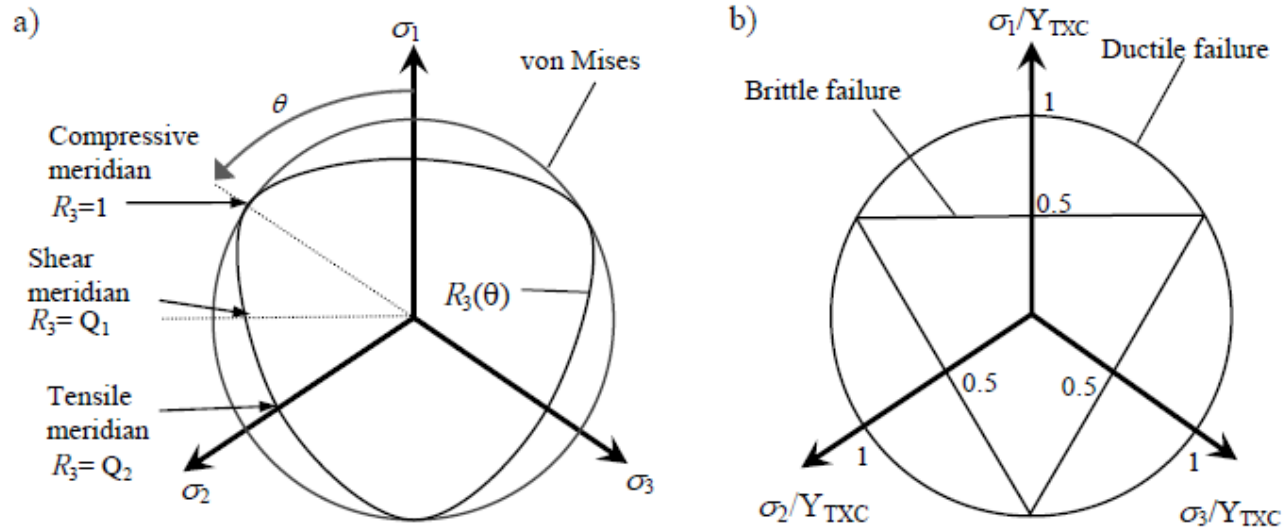

Figure 4. *Cross section through the failure surface at a deviatoric plane, modified from [4].*

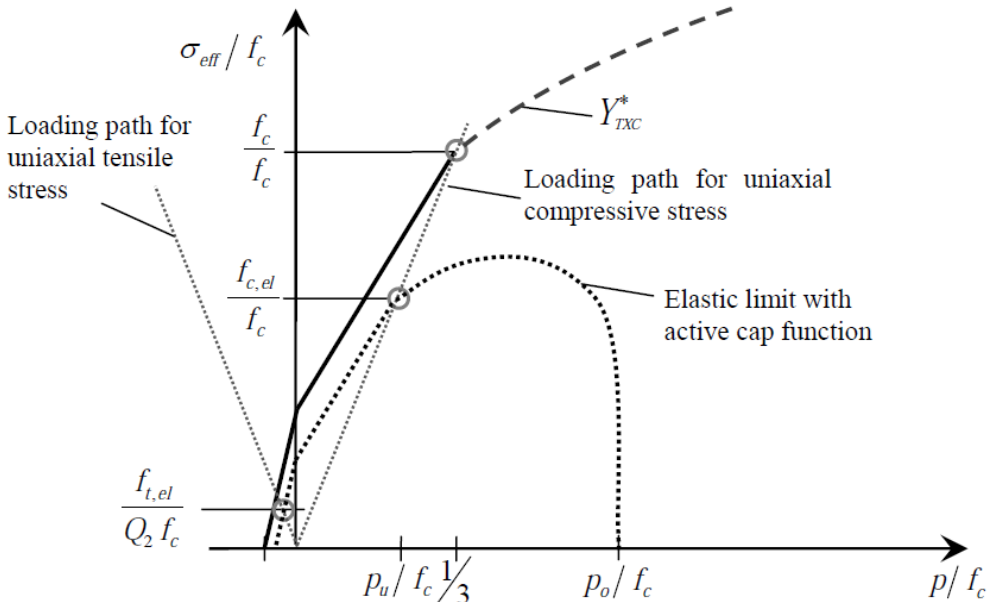

Figure 5. *A schematic figure of the elastic limit, modified from [4]*

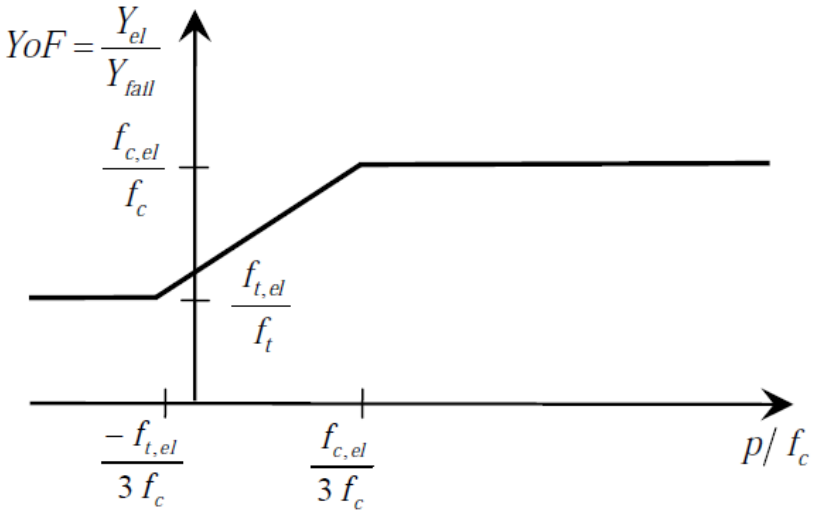

Figure 6*. The pressure dependent scale function for the ratio between elastic and failure strength surfaces, modified from [4].*

Linear strain hardening is used between the elastic and failure surfaces, and hardening modulus is given by the input ratio $G_{el}(G_{el}\text{-}G_{pl})$ (Century Dynamics, 2005b), which defines the ratio between the original shear modulus and the hardening modulus. The elastic strength surface is then defined as:

$$Y_{el}(p,\theta,\dot{\varepsilon}) = Y_{fail}(p,\theta,\dot{\varepsilon}) Y_0 FF_{Cap}(p) \qquad \textbf{(6)}$$

Furthermore, the elastic part of the deformation decreases at high pressures and the option to use a cap on the elastic surface ensures that the elastic surface closes at high pressures. The elastic strength surface within the RHT material model can be forced to close at high pressures by activation of

dimensionless cap function $F_{Cap}(p)$, which goes smoothly from unity to zero. The cap function is unity up to the pressure p_u where the uniaxial compression path intercepts with the elastic surface. At higher pressures $F_{Cap}(p)$ decreases and reaches zero at the pressure p_0, which is obtained as p_{crush} from the P-α EOS input data. The mathematical expression for $F_{Cap}(p)$ is given as:

$$\begin{cases} 1 & for \quad p \le p_u \\ \sqrt{1-\left(\dfrac{p-p_u}{p_0-p_u}\right)^2} & for \quad p \le p \le p_0 \\ 0 & for \quad p_0 \le p \end{cases} \tag{7}$$

The damage in the material grows after the stress point passes the failure surface according to:

$$D = \sum \frac{\Delta \varepsilon_{pl}}{\varepsilon_{pl}^{failure}} \tag{8}$$

$$\varepsilon_{pl}^{failure} = D_{RHT1}\left(p^* - p_{spall}{}^*\right)^{D_{RHT2}} \ge \varepsilon_{PL,\min}^{failure} \tag{9}$$

with D_{RHT1} and D_{RHT2} taken as material specific parameters.

At low pressures, a lower limit of the failure strain is set by introducing a minimum failure strain $\varepsilon_{\min}^{failure}$, with the damage evolution calibrated for cyclic uniaxial compressive stress conditions according to Holmquist et al. [9]. The residual strength Y_{fric}^* (normalised to the unconfined compression strength) of the fully damaged concrete is calculated from Eq. 4.40a, with the Autodyn notation given in *Eq. 10b* [10].

$$Y_{fric}^* = B_{fric} \times \left(p^*\right)^{N_{fric}} \qquad [4] \tag{10a}$$

$$Y_{fric}^* = B \times \left(p^*\right)^{M} \qquad [10] \tag{10b}$$

The strength is interpolated from the strength values for the undamaged material (D=0) at the failure surface and the completely damaged material (D=1) according to:

$$G_{fractured}(D) = D_{D=0}(1-D) + G_{D=1} \times D \text{ with } G_{D=1} = ShratD \times G_{D=0}$$

In *Figure 7* characteristics of the RHT model are schematically shown. The input parameters for the RHT material model for NSC are given in *Table 1* [4], with modifications for the parameter set for the 48 MPa NSC shown. Furthermore, the base parameter set for the HPC with 92 MPa concrete strength is also shown. Data from confined GREAC tests of this HPC were used for

calibration of this parameter set (Hansson, 2001, [14]), with an alternative parameter set presented by Svinsås et al. [15].

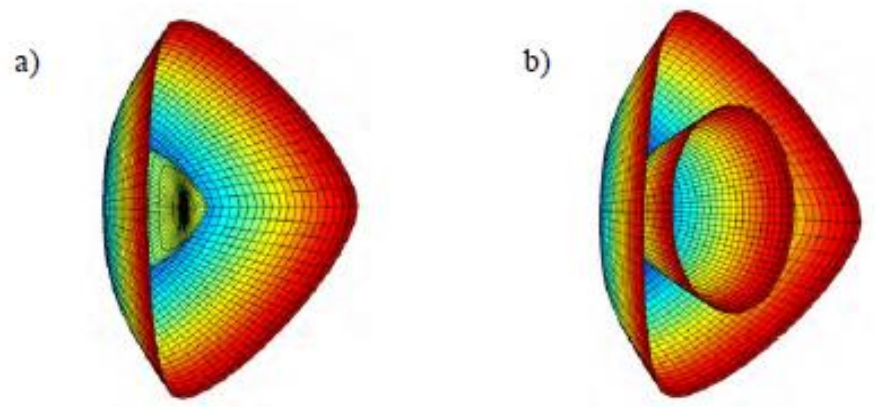

Figure 4.15. *Figure (a) shows the failure surface (outer) and the elastic limit surface (inner),with figure (b) showing the failure surface (outer) and the residual strength surface (inner).*

Table 1. *RHT strength model parameters for 35 MPa normal strength concrete according to Riedel (2000), and modified base parameter set used for concrete types with 48 and 92 MPa strengths.*

Parameter	NSC, 35 MPa (Reidel [4])	NSC, 48 MPa (Hansson, [16])	HPC, 92 MPa (Hansson, [14])
G_{el} *(GPa)*	*16.7*	*16.7*	*18*
f_c *(MPa)*	*35*	*48*	*92*
f_t/f_c	*0.10*	*0.083*	*0.057*
f_s/f_c	*0.18*	*0.18*	*0.30*
A_{fail}	*0.00*	*0.00*	*0.00*
B_{fail}	*1.60*	*1.60*	*1.90*
$Q_{2.0}$	*0.6805*	*0.6805*	*0.6805*
BQ	*0.0105*	*0.0105*	*0.0105*
$G_{el}/(G_{el}-G_{pl})$	*2.00*	*2.00*	*2.00*
$f_{t,el}/f_t$	*0.70*	*0.70*	*0.80*
$f_{c,el}/f_c$	*0.53*	*0.53*	*0.53*
Cap option	*Active*	*Active*	*Active*
B_{fric}	*1.60*	*1.60*	*1.60*
N_{fric}	*0.61*	*0.61*	*0.61*
α	*0.032*	*0.032*	*0.010*
δ	*0.036*	*0.036*	*0.013*
D_{RHT1}	*0.04*	*0.04*	*0.08*
D_{RHT2}	*1*	*1*	*1*
$\varepsilon_{\min}^{failure}$	*0.01*	*0.01*	*0.05*
ShartD	*0.13*	*0.13*	*0.13*

3. Conclusion

The RHT material model has a comprehensive framework that encompasses many important features of concrete-like brittle materials under high impulsive loading. However, numerical tests indicate that this material model, as implemented in AUTODYN, falls short in representing the concrete behavior under certain loading conditions, particularly concerning the tension response and softening behavior. To a certain extent, these problems may be corrected by appropriately determining the influencing model parameters. Numerical simulation of penetration of concrete targets by steel projectile is conducted to further evaluate the performance of the modified RHT model in real applications. The results from simulations of a series of physical penetration/perforation experiments demonstrate appreciable improvements in the damage patterns, as well as in the predicted parameters including the depth of penetration, projectile exit velocity and the size of the crater.

5. Acknowledgements

This paper has been financially supported within the project entitled "Horizon 2020 - Doctoral and Postdoctoral Studies: Promoting the National Interest through Excellence, Competitiveness and Responsibility in the Field of Romanian Fundamental and Applied Scientific Research", contract number POSDRU/159/1.5/S/140106. This project is co-financed by European Social Fund through Sectoral Operational Programme for Human Resources Development 2007- 2013. Investing in people!

References

[1] UNOSSON M, NILSSON L. *Projectile penetration and perforation of high strength concrete: experimental results and macroscopic modeling.* Int. J Impact Eng 2006;32:1068-85.

[2] NILSSON L. *Impact loading on concrete structures: a constitutive modelling, finite element analysis, and experimental study of nonlinear wave propagation*. Doctoral thesis, Chalmers University of Technology, Goteborg, Sweden; 1979.

[3] CHEN W.F. *Plasticity in Reinforced Concrete*. New York: McGraw Hill; 1982.

[4] RIEDEL W, THOMA K, HIERMAIER S. *Penetration of reinforced concrete by BETA-B-500--numerical analysis using a new macroscopic*

concrete model for hydrocodes. Proceedings of 9th International Symposium on Interaction of the Effect of Munitions with Structures. 1999. p.315-22.

[5] RIEDEL W, KAWAI N AND KONDO K. *Numerical Assessment for Impact Strength Measurements in Concrete Materials*, International Journal of Impact Engineering 36 (2009), pp. 283-293.

[6] RIEDEL W. *Beton unter dynamischen Lasten: Mesound makromechanische Modelle und ihre Parameter*, Ed.: Fraunhofer EMI/IRB, Freiburg 2004, ISBN 3-8167-6340-5.

[7] MALVAR LJ, CRAWFORD JE, WESEVICH JW, SIMONS D. *A plasticity concrete material model for DYNA3D*. Int J Impact Eng. 1997; 19(9-10): 847-73.

[8] MALVAR L J, CRAWFORD JE, MORRILL KB. *K&C concrete material model Release III - Automated generation of material model input.* K&C technical report TR-99-24-B1; August 18, 2000

[9] HOLMQUIST TJ, JOHNSON GR, COOK WH. *A computational constitutive model for concrete subjected to large strains, high strain rates, and high pressures.* 14th International Symposium on Ballistics. Quebec, Canada; 1993. p.591-600.

[10] Century Dynamics, *Autodyn release notes, Version 4.2,* Century Dynamics, Horsham, 2005b.

[11] CEB, *CEB-FIP model code 1990*, published by Thomas Telford for the Comité Euro-International du Béton, ISBN 0-7277-1696-4, London, 1993.

[12] LI, Q.M. AND MENG, H., *About the dynamic strength enhancement of concrete-like materials in a split Hopkinson pressure bar test*, International Journal of Solids and Structures, Vol. 40, No 2, 2003, pp. 343-360.

[13] WILLIAM, K.J. AND WARNKE, E.P., *Constitutive model for the triaxial behavior of concrete,* Seminar on concrete structure subjected to triaxial stresses, Bergamo, 17th - 18th May 1974, Int. Association of Bridge and Structural Engineers Proceedings, Vol. 19, Session no. III, paper

[14] HANSSON, H., *Numerical simulation of concrete penetration with Euler and Lagrange formulations,* Swedish Defence Research Agency, report no. FOI-R--0190--SE, Tumba, September 2001.

[15] SVINSÅS, E., O'CARROLL, C., WENTZEL, C. M. AND CARLBERG, A., *Benchmark trial designed to provide validation data for modelling.* Proc. of the 10th International Symposium on Interaction of the Effects of Munitions with Structures, San Diego, 7th - 11th of May 2001.

[16] HANSSON, H., *Warhead penetration in concrete protective structures,* Licentiate Thesis Stockholm, October 2011